Biomaterials 317 (2025) 123047

Contents lists available at ScienceDirect

Biomaterials

journal homepage: www.elsevier.com/locate/biomaterials

Targeted LNPs deliver IL-15 superagonists mRNA for precision cancer therapy

Juntao Yu [a,1], Qian Li [b,1], Chaoting Zhang [d], Qiu Wang [b], Shenggen Luo [a], Xiaona Wang [a], Rongkuan Hu [a,**], Qiang Cheng [b,c,*]

[a] Starna Therapeutics Co., Ltd., Suzhou, 215123, China
[b] Department of Biomedical Engineering, College of Future Technology, Peking University, Beijing, 100871, China
[c] Beijing Advanced Center of RNA Biology (BEACON), Peking University, Beijing, 100871, China
[d] Key Laboratory of Carcinogenesis and Translational Research (Ministry of Education/Beijing), Laboratory of Biochemistry and Molecular Biology, Peking University Cancer Hospital and Institute, Beijing, 100142, China

ARTICLE INFO

Keywords:
IL-15 superagonists
mRNA delivery
Lipid nanoparticles
Lung-targeting
Cytokine therapy

ABSTRACT

Interleukin-15 (IL-15) emerges as a promising immunotherapeutic candidate, but the therapeutic utility remains concern due to the unexpected systematic stress. Here, we propose that the mRNA lipid nanoparticle (mRNA-LNP) system can balance the issue through targeted delivery to increase IL-15 concentration in the tumor area and reduce leakage into the circulation. In the established Structure-driven TARgeting (STAR) platform, the LNP^{Local} and LNP^{Lung} can effectively and selectively deliver optimized IL-15 superagonists mRNAs to local and lungs, respectively, in relevant tumor models. As a result, such superagonists exhibited well-balanced efficacy and side-effects, demonstrating the better anti-tumor activity, less systematic exposure, and less cytokine related risks. We finally verified the selective delivery and well tolerability of LNP^{Lung} in non-human primates (NHPs), confirming the potential for clinical application. This finding provides new potentials for cancers treatment on lung cancers or lung metastasis cancers.

1. Introduction

The critical role that Interleukin-15 (IL-15) plays in innate and adaptive immunity has had profound implications in the field of immunology [1,2]. The biological effects of IL-15 are mediated through interaction with a receptor complex comprising three distinct chains: CD122 (IL-2/IL-15Rβ), CD132 (IL-2/IL-15Rγc), and the high-affinity-specific chain IL-15Rα [3]. Currently, IL-15 has garnered considerable attention as a promising immunotherapeutic candidate for cancer treatment [4,5], exemplified by the advancement of the IL-15 analogue and agonist complex agent nogapendekin alfa (N-803) [6–9], as well as the ongoing clinical trials of similar agents [10–12]. However, potential side effects still remain due to the mechanism by which IL-15 superagonists activate T/NK cells [13–15]. Such potential adverse effects was believed from the shared activities of IL-15 and IL-2, evidenced by the increase in IL-15 in autoimmune disorders [16], and high level of IL-15/IL-15Rα positively associated with leukemia [17–20]. During the treatment process, therapeutic enhancement of CD8 T cells, NK cells, and in some cases CD4 T cells was observed at all doses and any routes of administration of IL-15 [21,22]. Of note, higher doses and frequent administrations not only result in more pronounced responses, but also cause clinical side effects such as anorexia, diarrhea, weight loss, and transient grade 3–4 neutropenia [23–26]. All these symptoms can be ascribed to the overreaction of immune system [27–32], which is the key mechanism for IL-15 exerts its efficacy. Moreover, the first indication for the N-803 approved by the Food and Drug Administration (FDA) for the treatment of bladder cancer was based on intravesical administration [33], which can relatively balance therapeutic efficacy and potential adverse effects compared with systemic injection. Likewise, we suppose that this balance could also be achieved through targeted delivery to endow maximum IL-15 concentration in the target area but reduce leakage into the circulation.

The mRNA technology may become one of the options for achieving the above goal via targeted delivery and expression. The success of

* Corresponding author. Department of Biomedical Engineering, College of Future Technology, Peking University, Beijing, 100871, China.
** Corresponding author.
E-mail addresses: hurongkuan@starnatx.com (R. Hu), qiangcheng@pku.edu.cn (Q. Cheng).
[1] These authors contributed equally to this work.

https://doi.org/10.1016/j.biomaterials.2024.123047
Received 26 September 2024; Received in revised form 10 December 2024; Accepted 23 December 2024
Available online 24 December 2024

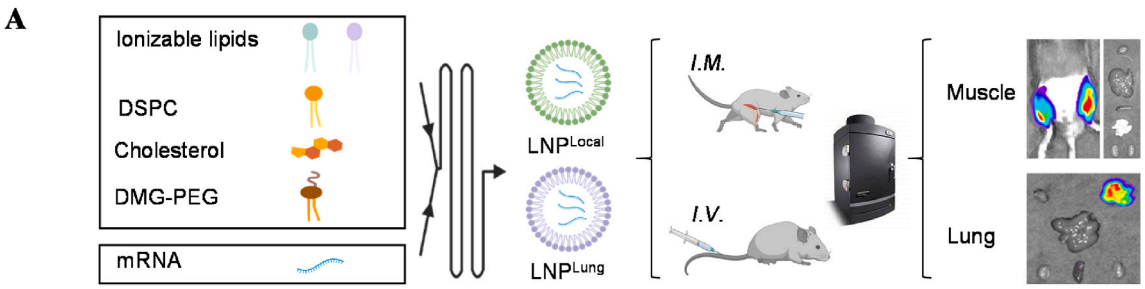

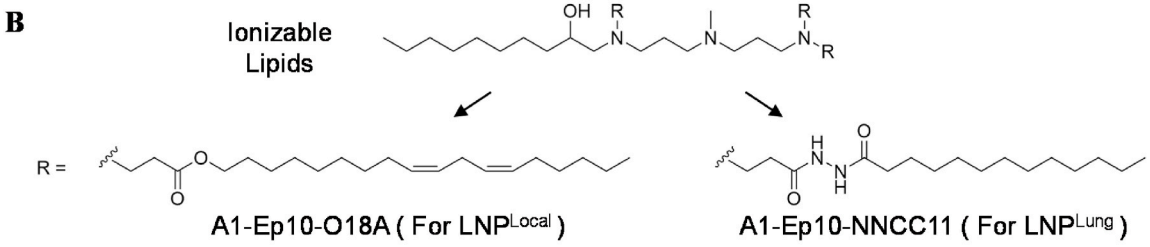

C

	Size (nm)	PDI	E.E.(%)
LNP^{Local}	84.93 ± 2.72	0.072 ± 0.013	94.72 ±3.58
LNP^{Lung}	53.23 ± 1.36	0.131 ± 0.026	99.77± 0.05

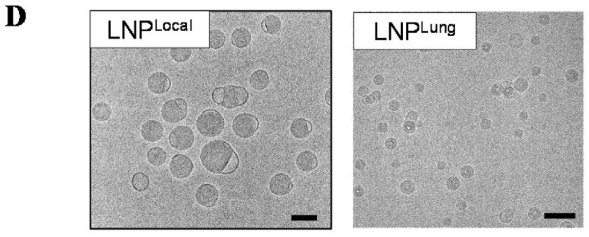

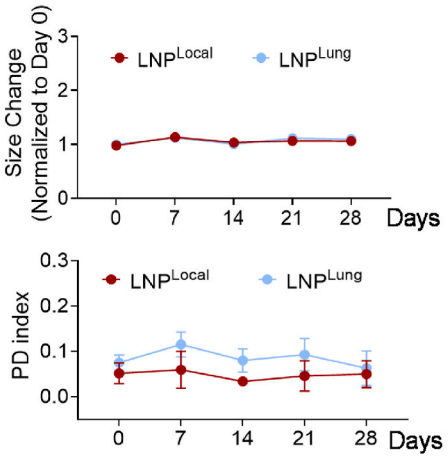

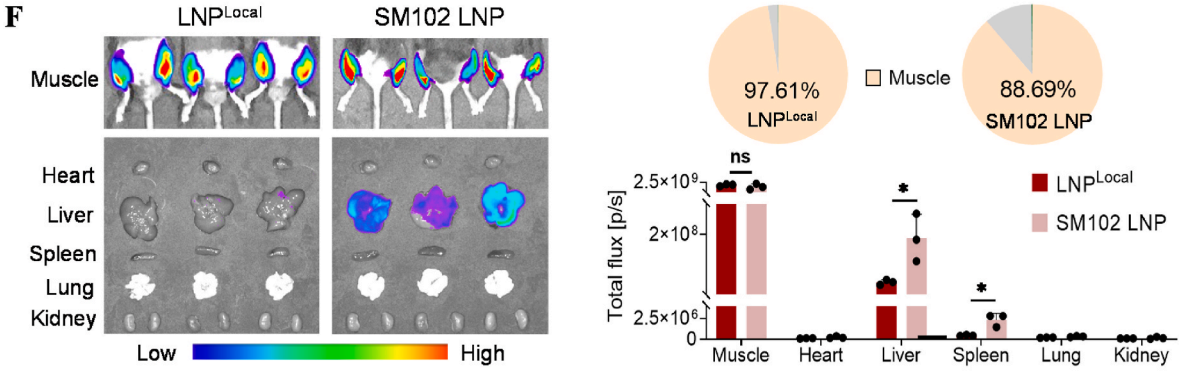

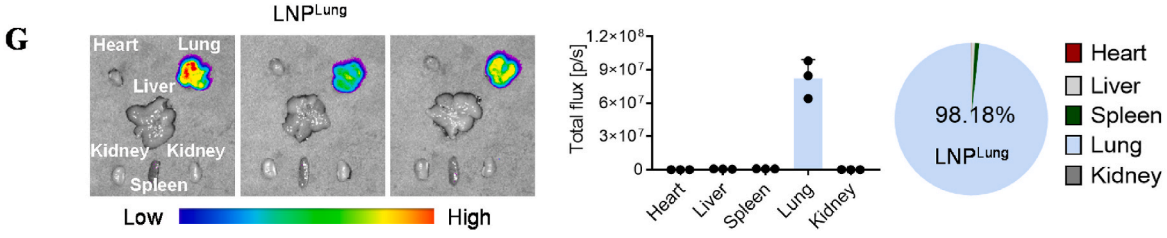

(caption on next page)

Fig. 1. The preparation and characterization of LNP^{Local} and LNP^{Lung}, and LNP specifically deliver mRNA to muscle and lung via local and intravenous administration. (A) Schematic diagram of LNP construction and targeted mRNA delivery to muscle and lung. **(B)** The chemical structures of ionizable lipids used in LNP^{Local} and LNP^{Lung}. **(C)** LNP^{Local} and LNP^{Lung} encapsulating Fluc mRNA possessed uniform particles with high encapsulation efficiency (>90 %), Data are presented as mean ± s.e.m. (n = 3, biologically independent samples). **(D)** Images of Cryo-electron microscopy showed that LNP^{Local} and LNP^{Lung} had similar morphology (Scale bar = 100 nm). **(E)** LNP^{Local} and LNP^{Lung} exhibited well stability at 4 °C over 28 days (n = 3 biologically independent samples). **(F)** LNP^{Local} significantly reduced liver leakage of mRNA compared to SM102 LNP via *i.m.* injection (0.05 mg/kg/leg). (G) Specific delivery of Fluc mRNA by LNP^{Lung} to lung via *i.v.* administration (0.25 mg/kg). The percentage and total flux of luciferase expression in muscles and other major organs were analyzed by living image software (n = 3 biologically independent animals). Data are shown as mean ± s.e.m. A two-tailed unpaired *t*-test was used to determine the significance of the comparisons of data indicated in F (n.s. no significance, $*P < 0.05$).

mRNA technology in COVID-19 vaccines has propelled it into a global research focus, marking a rapid advancement [34]. Through sequence design, mRNA can encode a wide range of proteins, offering extensive application prospects [35–39]. Delivered through lipid nanoparticles (LNP), mRNA technology has been successfully applied to the defense and treatment of multiple diseases, making this delivery platform one of the most important factors in clinical translation [40–46]. However, targeted delivery of mRNA-LNP to specific organs and cells remains challenging, which could be partially satisfied by high-throughput screening, component optimization, and antibody modification [41, 47–54]. Through rational design, we previously have synthesized hundreds of ionizable cationic lipids and established a Structure-driven TARgeting (STAR) platform, in which tissue-selective mRNA-LNP was fully validated (PCT/CN2023/137998). Notably, LNP^{Local} and LNP^{Lung} from STAR LNPs library could specifically deliver mRNA into local tissues and lungs, respectively, which may meet the needs of tumor therapy by delivering mRNA encoding IL-15 superagonists, especially in designed tissues.

To this end, we firstly evaluated the structural activity of IL-15 superagonist mRNAs. The STR-2 mRNA, designed proteins from N-terminal to C-terminal of immunoglobulin G Fc fragment, IL-15Rα sushi domain, and IL-15, showed superior efficacy compared to the benchmark N-803. Then, sequence-optimized mRNAs (STR-2-D43 and STR-2-D61) with aspartic acid mutations were verified in subcutaneous and lung metastasis tumor models. In multiple mice model, the optimal IL-15 superagonist mRNAs delivered by LNP^{Local} via intratumoral and LNP^{Lung} via intravenous injection, could significantly inhibit tumor growth. Moreover, the mRNA-LNP system minimized IL-15 leakage to major organs, reducing adverse effects such as weight loss and cytokine-related immune activation. More importantly, the mRNA-LNP^{Lung} exhibited excellent delivery efficiency and biosafety in non-human primates, demonstrating great potential for clinical translation. These findings suggest that targeted mRNA-LNPs offer a promising option for IL-15-based cancer treatment, especially for lung cancers and metastatic tumors.

2. Materials and methods

A detailed description of the materials and methods involved in this study is provided in the Supplemental Information.

3. Results

3.1. Validation of targeted mRNA-LNPs

To improve the therapeutic window of IL-15, we propose that mRNA-LNP system may satisfy the goal via targeted delivery. On the one hand, the structure and sequence of IL-15 superagonists can be refined and optimized in the form of mRNA to enhance their anti-tumor activity. Targeted LNPs, on the other hand, could satisfy limited higher concentrations of IL-15 around the tumor area but minimize leakage into the circulation to reduce unintended side effects. We previously synthesized a library of ionizable cationic lipids through rational design for mRNA-LNP targeted delivery, named Structure-driven TARgeting (STAR). Among them, two distinct lipids, A1-Ep10-O18A and A1-Ep10-NNCC11 (Scheme S1-S2, Figs. S1–S4) were endowed to form LNP and mediate high efficacy and specificity for local (LNP^{Local}) and lung (LNP^{Lung}) mRNA delivery through local and intravenous (i.v.) injection, respectively (Fig. 1A and 1B).The particle size of LNP^{Local} was 84.93 ± 2.72 nm, and that of LNP^{Lung} was 53.23 ± 1.36 nm, both with uniform polydispersity index (PDI), and the encapsulation efficiency (EE) was determined to be 94.72 % ± 3.58 % and 99.77 % ± 0.05 %, respectively (Fig. 1C). The Cryo-TEM images revealed a highly consistent morphology for both LNP^{Local} and LNP^{Lung} samples (Fig. 1D). Furthermore, stability testing indicated negligible changes in particle size and PDI for both LNPs after 28 days of storage at 4 °C (Fig. 1E), affirming their substantial stability and suitability for *in vivo* investigations. Through local injection, intramuscular (i.m.), mRNA-LNP^{Local} exhibited enhanced efficiency and reduced hepatic leakage compared with commercial FDA-approved SM102 LNP (Fig. 1F), that the percentage of muscle expression was 97.61 % for LNP^{Local} and 88.69 % for the SM102 LNP. These results convincingly demonstrated that LNP^{Local} enhanced local targeting and reduced hepatic extravasation after local injection. Similarly, through i.v. delivery, the expression of firefly luciferase (Fluc) was identified in the lungs by mRNA-LNP^{Lung} (Fig. 1G). Bioluminescence in the lungs accounted for 98.18 % of overall bioluminescence, with negligible leakage (0.71 %) in the liver. Such result underscores the remarkable ability of LNP^{Lung} to specifically target the lungs. Overall, the results indicated that both LNP^{Local} and LNP^{Lung} had the potential to specifically deliver IL-15 superagonist mRNA in desired tissues.

3.2. The structural optimization of mRNA encoding IL-15 superagonist

The sushi domain of IL-15Rα has been recognized for stabilizing IL-15 [55], by which the N-803 was approved by the FDA in 2024 [33]. Despite this achievement, the structural organization of the IL-15-IL-15Rα complex still leaves room for improvement. To address this, we established distinct structures for IL-15-IL-15Rα (sushi) complexes (IL-15 superagonists) (Fig. 2A). In the IL2Rbeta-STAT5 based luciferase-reporter system, TF-1 cells were co-cultured with cell medium containing either N-803 or secreted IL-15 superagonists, and the luminescence was detected post 24 h (Fig. 2B). The data revealed that STR-2 (C-terminal IL-15) exhibited reduced EC50 values than N-803 and STR-1 (C-terminal Fc) (Fig. 2C). Considering IL-2Rβ-STAT5 signaling is the key signaling pathway of IL-15 downstream activation in its target cell–lymphocytes [56], this result indicated that STR-2 might have better potency than N-803. This was supported by subsequent data derived from peripheral blood mononuclear cells (PBMCs) of both lung cancer patients and healthy individual (Fig. 2D–F). After co-cultured with STR-2 supernatant (Fig. 2D), a significantly elevated level of pSTAT5 and interferon gamma (IFNγ) was observed (Fig. 2E and 2F). In addition, both STR-1 and STR-2 supernatant groups presented a significant elevated proliferation rate than N-803 group (Fig. 2G), indicating an excellent activity enhancement of mRNA modality. Moreover, the proliferation of target cells ($CD8^+$ T and $CD56^+$ NK cells) was observed in all treated groups, with STR-2 appearing to be better (Fig. 2H and 2I). These findings suggested that structural optimization of IL-15 superagonist was critical, and C-terminal IL-15 design was more attractive.

3.3. The anti-tumor efficacy of STR-2 in subcutaneous tumor models

To further test the anti-tumor activity of STR-2, we applied mRNA-

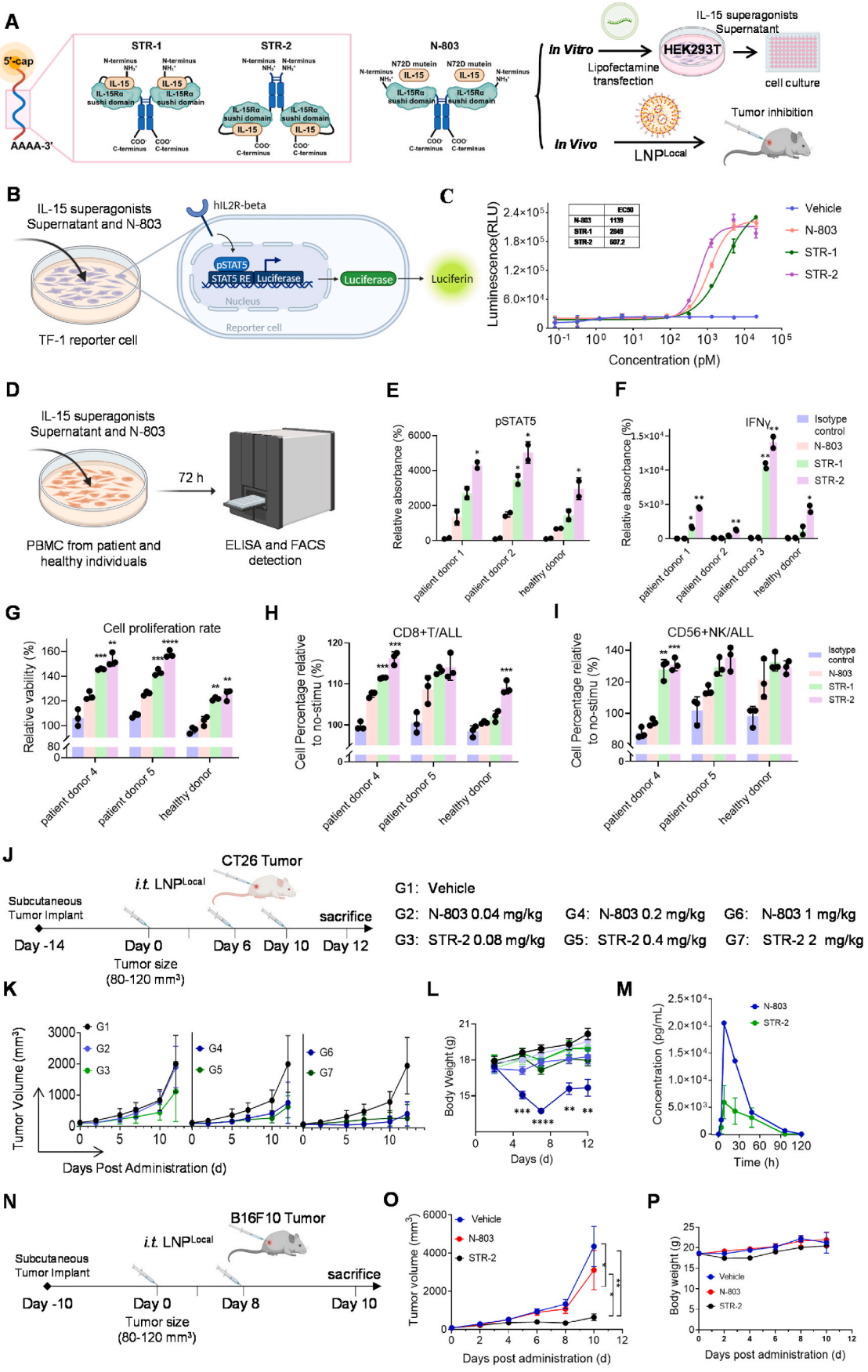

(caption on next page)

Fig. 2. Structural optimization of mRNA encoding IL-15 superagonists to achieve superior antitumor effects. (A) A schematic illustration depicting the structural optimization and validation procedure of IL-15 superagonists. **(B)** Schematic diagram of IL-15 signaling reporter cell (IL-2Rβ-STAT5 signaling TF-1 reporter cell) design. **(C)** The lower EC50 value indicated that STR-2 activated more effectively the IL-2Rβ-STAT5 signal in TF-1 cells compared to N803 and STR-1. **(D)** Schematic diagram of sample preparation for *in vitro* activity testing of IL-15 superagonists. **(E–F)** IL-15 superagonists significantly elevated the levels of pSTAT5 **(E)** and IFNγ **(F)** of PBMC from both lung cancer patients and healthy individual after co-culture for 72 h. (G–I) STR-1 and STR-2 effectively promoted the overall **(G)**, $CD8^+$ T cell **(H)** and $CD56^+$ NK cell **(I)** proliferation of PBMC from both lung cancer patients and healthy individuals (N-803: 4.5 nM, mRNA-encoded IL-15 superagonists: 0.1 nM). **(J)** Schematic representation of anti-tumor effects by STR-2 LNP^{Local}. Tumor growth curves **(K)** and body weight change profiles of mice **(L)** were employed to access anti-tumor efficacy and bio-safety, respectively. Data are presented as mean ± s.e.m. (n = 5 biologically independent animals). **(M)** Pharmacokinetic profiles demonstrated that N-803 had lager AUC than STR-1, revealing more leakage of N-803 in circulation. Data are shown as mean ± s.e.m. (n = 5 biologically independent animals). **(N)** The schematic diagram of optimized mRNA STR-2 for treating B16F10 tumor by LNP^{Local}. **(O)** Compared with vehicle and N-803, STR-2 remarkably inhibited tumor growth of mice (vehicle: empty LNP, N-803: 0.2 mg/kg, SRT-2: 2 mg/kg; *i.t.* on day 0 and day 8). Data are illustrated as mean ± s.e.m. (n = 5 biologically independent animals). **(P)** Average body weight of bearing-tumor mice on day 0–10. Data are presented as mean ± s.e.m. (n = 5 biologically independent animals). A two-tailed unpaired *t*-test was used to determine the significance of the comparisons ($^*P < 0.05$; $^{**}P < 0.01$; $^{***}P < 0.001$; $^{****}P < 0.0001$).

LNP^{Local} delivery system in subcutaneous heterotopic tumor models (Fig. 2J). Through intratumoral (i.t.) injection, STR-2 exhibited similar efficacy in inhibiting tumor growth compared to the group treated with N-803 in the CT26 tumor model, and the anti-tumor effect was dose-dependent (Fig. 2K, Fig. S5A, and Table S1). Importantly, the N-803 group displayed significant reduction in body weight at high dose (1 mg/kg), and the mean animal weight loss was nearly 20 %, whereas mRNA-LNP groups maintained consistent body weight cross all tested doses (Fig. 2L). Given that rapid weight loss was a reliable predictor of clinical deterioration, many institutional animal care and use committees adopted the recommendation to consider euthanasia for animals that loss 20 % of their body weight [57], this result indicated systemic distress and significant sickness in N-803 group at high dose. It is worth mentioning that the dosage of mRNA-LNP (2 mg/kg) was twice that of N-803 (1 mg/kg), revealing the well-balanced efficacy and systematic stress *in vivo* via mRNA modality. Pharmacokinetics studies demonstrated that N-803 group (0.2 mg/kg) had higher drug concentrations in the plasma and larger area under the curve (AUC) compared to the 10 times higher dose mRNA-LNP groups (2 mg/kg) (Fig. 2M), which was believed to resulted in side effects associated with systemic exposure to IL-15 superagonists. Again, the superior anti-tumor efficacy of STR-2 was further supported in the B16F10 tumor model (Fig. 2N and 2O). Herein, dose of 0.2 mg/kg N-803 was used due to systematic stress. As expected, no significant decrease in body weight was observed in the 10-fold higher dose (2 mg/kg) of the mRNA groups (Fig. 2P), and showed more pronounced efficacy in inhibiting tumor growth (Fig. S5B, and Table S2).

3.4. Sequence optimization of mRNA encoding STR-2

Previously study reported that mutating amino acid (AA) into aspartic acid (Asp, D) in IL-15 agents could potentially improve its receptor binding affinity and downstream signaling activity [58], which inspired us to further optimize the sequence of STR-2 for seeking better efficacy. We first performed codon optimization on STR-2 and obtained STR-2-D0 (without D mutation). A series of mutated STR-2 sequences were then generated by one-by-one "to D″ AA mutation from the N-terminus to the C-terminus in the IL-15 portion, resulting in 108 different mutants (Fig. 3A, Table S3). For example, STR-2-D61 indicates that the 61st not-D-AA of the IL-15 portion is mutated to D. Then the 108 mutants were evaluated to initiate IL-2Rβ-STAT5 signaling in reporter cells. Five of them (STR-2-D43, STR-2-D56, STR-2-D61, STR-2-D65 and STR-2-D106) showed strong ability (Fig. 3B, Fig. S6, and Table S4). Furthermore, all the five variants showed similar or better binding affinity to IL-2Rβ/γ complex compared to STR-2-D0 (Fig. S7), indicating a potential 'enrichment to target' capability. All of them demonstrated better activity than N-803 in inducing proliferation of $CD8^+$ T cells and NK cells subclasses in PBMCs co-culture system, with the STR-2-D61 showed the best (Fig. 3C). We also noticed that STR-2-D43 showed moderate activity in reporter cells and PBMC *in vitro* activation, but the highest expression level in the HEK293T (Fig. S8), suggesting that it may be able to satisfy the anti-tumor activity at lower dosage of mRNA for potentially reducing a formulation related systematic stress.

Then, we tested the *in vivo* anti-tumor activity of STR-2-D61 and STR-2-D43 delivered by LNP^{Local}. The experiments were performed using subcutaneously transplanted MC38 tumor model in C57BL/6 mice. When tumors reached a volume range of 80–120 mm^3, the mice were randomly grouped and i.t. administered on specific days (day 0, day 3, day 7, day 10, and day 14) (Fig. 3D). N-803 showed limited effectiveness in inhibiting tumor growth, whereas the mRNA-encoding groups exhibited significant antitumor activity (Fig. 3E and 3H). No statistically reduction of body weight was observed, indicating the well-tolerated property (Fig. 3F). To illustrate the superiority of mRNA-LNP modality more clearly, we analyzed several blood indicators in tumor-bearing mice. Although N-803 treatment presented confined anti-tumor activity, the increasing level of the total number of white blood cells, IL-6 levels, eosinophils, and basophil subpopulations were significantly observed (Fig. 3G, and Fig. S9). Considering lymphocytes contribute to most of the IL-15 related anti-tumor activity [59] and IL-6 was one of the key factor to cytokine related side effects and the main factor in cytokine storm [60,61], these phenomena may explain why mRNA-LNP group presented restricted side effect compared with N-803 treatment group *in vivo*. Furthermore, the levels of red blood cells, hemoglobin, and platelets in the mRNA-LNP groups were all detected within the normal range (Fig. S10), verifying the hematological safety of this strategy.

3.5. IL-15 mRNA-LNP^{Lung} well-balanced the safety and anti-tumor efficacy

To further expand the antitumor potential of IL-15 mRNA-LNP approach, we intend to investigate the possibility of systemic delivery, which is very challenging due to uncontrollable side effects of IL-15 related agents mentioned above. First, we analyzed the leakage of IL-15 when i.v. delivered using the mRNA-LNP approach (Fig. 4A). The STR-2-D61 mRNA was delivered by LNP^{Lung} and LNP^{Liver}, respectively. We here named LNP^{Local} administered via intravenous injection as LNP^{Liver} because LNP^{Local} can mediate liver-targeted mRNA delivery upon intravenous injection (Fig. S11). Then serum protein concentrations were detected. Four hours post injection, an extremely high concentration (~2×10^5 pg/mL) of IL-15 was detected in the plasma from STR-2-D61 LNP^{Liver} group, and then the concentration was maintained over 100 h. As contrast, the protein concentration was below the limit of detection (50 pg/mL) 24 h after injection in the plasma of STR-D61 LNP^{Lung} group, and the peak concentration was very low (~2×10^3 pg/mL). Further detection of Comprehensive Metabolic Panel (CMP) presented that an increased blood level of aspartate transaminase (AST) and alanine transaminase (ALT) in LNP^{Liver} group was observed (Fig. 4B and 4C). AST and ALT are released into the bloodstream when hepatocytes are injured or die (as in cases of hepatitis). The elevated levels of either enzyme are the most common abnormalities observed in liver induced by IL-15 [62]. Moreover, the Hematoxylin and eosin (H&E) staining demonstrated that LNP^{Liver} group had portal inflammation with

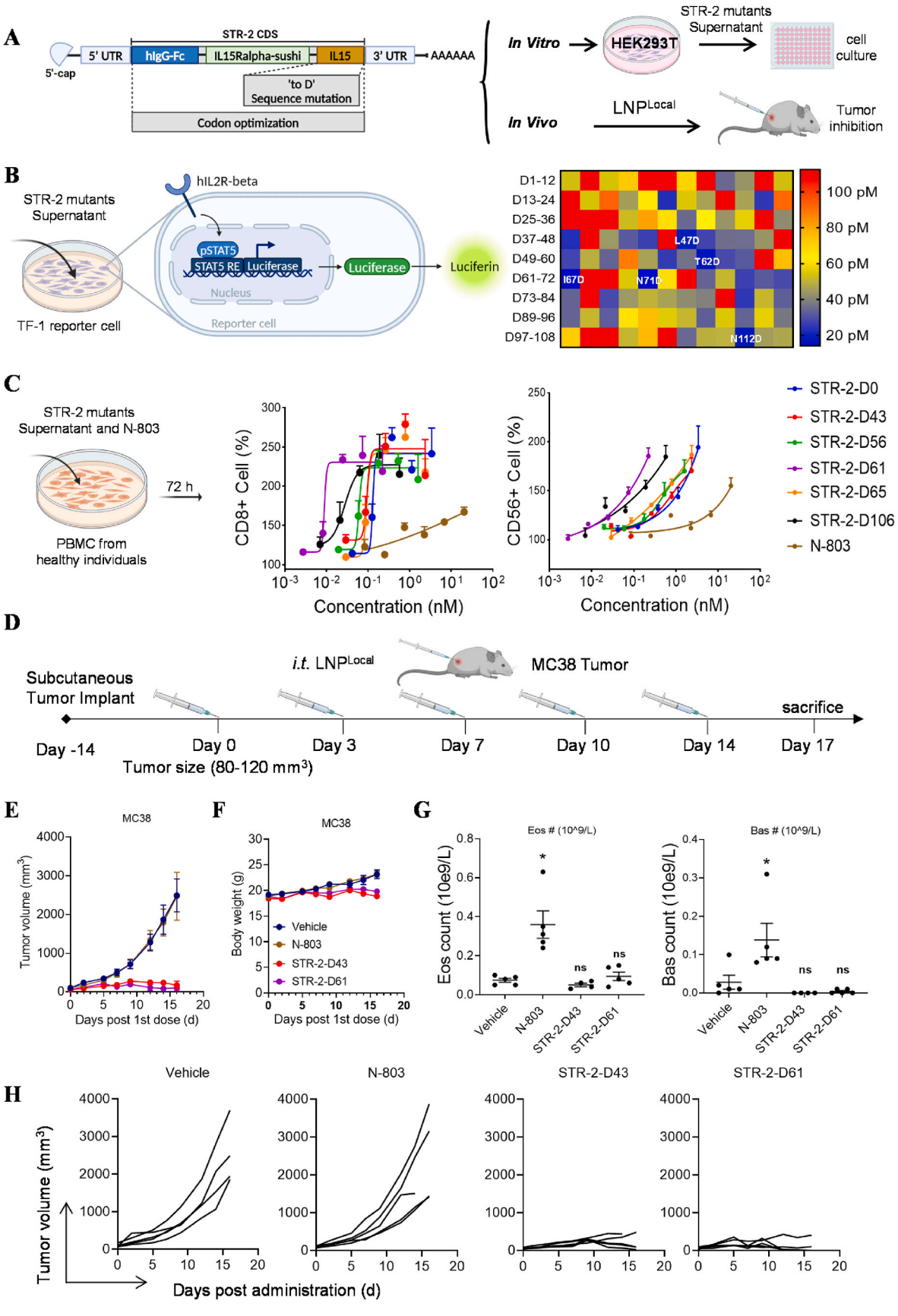

(caption on next page)

Fig. 3. Further optimized sequence of mRNA to enhance the antitumor efficacy. (A) The schematic illustration of STR-2 mRNA sequence optimization and evaluation. **(B)** The schematic diagram for assessing the activation ability of IL2Rβ-STAT5 signal in TF-1 reporter cells, as well as the EC50 heat map of 108 different STR-2 mutants generated by one-by-one "to D″ AA mutation. **(C)** Top STR-2 mutants exhibited stronger ability to induce $CD8^+$ T and NK cells proliferation than N-803. Data are presented as mean ± s.e.m. (n = 5 biologically independent samples). **(D)** The schematic representation of STR-2-D43 and STR-2-D61 mRNAs delivered by LNP^{Local} to assess the anti-tumor effects in MC38-tumor bearing mice. Tumor growth profiles **(E,H),** body weight change **(F)**, and Complete Blood Count **(G)** revealed that mRNA-LNP modality had remarkable antitumor advantages and better bio-safety (vehicle: empty LNP, *i.t.,* N-803: 0.2 mg/kg, *i.v.,* STR-2-D43: 2 mg/kg, *i.t.,* STR-2-D61: 2 mg/kg, *i.t.,* administration on day 0, 3,7,10 and 14). Data are shown as mean ± s.e.m. (n = 5 biologically independent animals). A two-tailed unpaired *t*-test was used to determine the significance of the comparisons (n.s. no significance, $^*P < 0.05$).

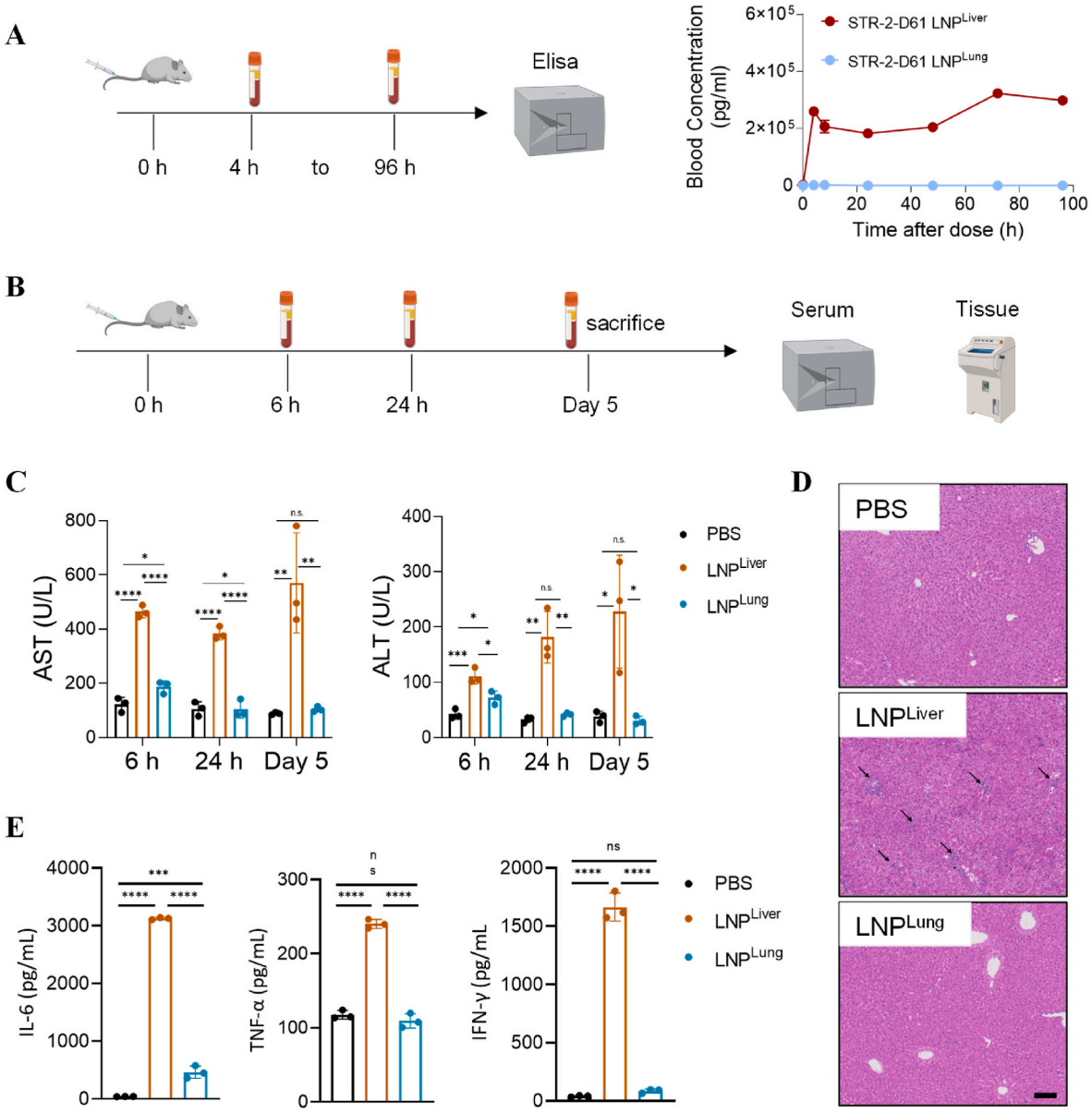

Fig. 4. IL-15 mRNA-LNP^{Lung} significantly improved the *in vivo* bio-safety of IL-15 by reducing its leakage in circulation. (A) Schematic illustration showed the process of mice administration, sampling and STR-2-D61 protein level evaluation. STR-2-D61 LNP^{Liver} exhibited higher protein level in blood compared to STR-2-D61 LNP^{Lung}, implying more leakage in circulation (*i.v.*). Data are presented as mean ± s.e.m. (n = 3 biologically independent animals). **(B)** Schematic presentation of *in vivo* bio-safety of LNP^{Liver} and LNP^{Lung}. The mice were administered *i.v.* with LNP^{Liver} and LNP^{Lung} encapsulating STR-2-D61 mRNA (1 mg/kg). **(C, D)** At 6 h, 24 h, and 5 days, the liver-toxicity was evaluated by measuring the levels of AST and ALT in serum, and H&E staining was applied to further estimate the liver injury. In the LNP^{Liver} i.v. treatment group, obvious portal inflammation accompanied with necrosis and lymphocyte infiltration was observed (arrows) (Scale bar = 100 μm). **(E)** The levels of inflammation cytokine (IL6, TNF-α and IFN-γ) in mice serum were detected by ELISA. Data are presented as mean ± s.e.m. (n = 3 biologically independent animals). A two-tailed unpaired *t*-test was used to determine the significance of the comparisons (n.s. no significance, $^*P < 0.05$; $^{**}P < 0.01$; $^{***}P < 0.001$; $^{****}P < 0.0001$).

piecemeal to moderate necrosis and lymphocytes infiltration in liver (Fig. 4D), affirming the pathologically damage. Besides, LNP^{Liver} significantly elevated the levels of inflammatory cytokines in the circulation, including IL-6, TNFα, and IFN-γ, but no noticeable change treated by LNP^{Lung} (Fig. 4E). All these results demonstrated that STR-2-D61 LNP^{Lung} might be able to balance the safety and efficacy in

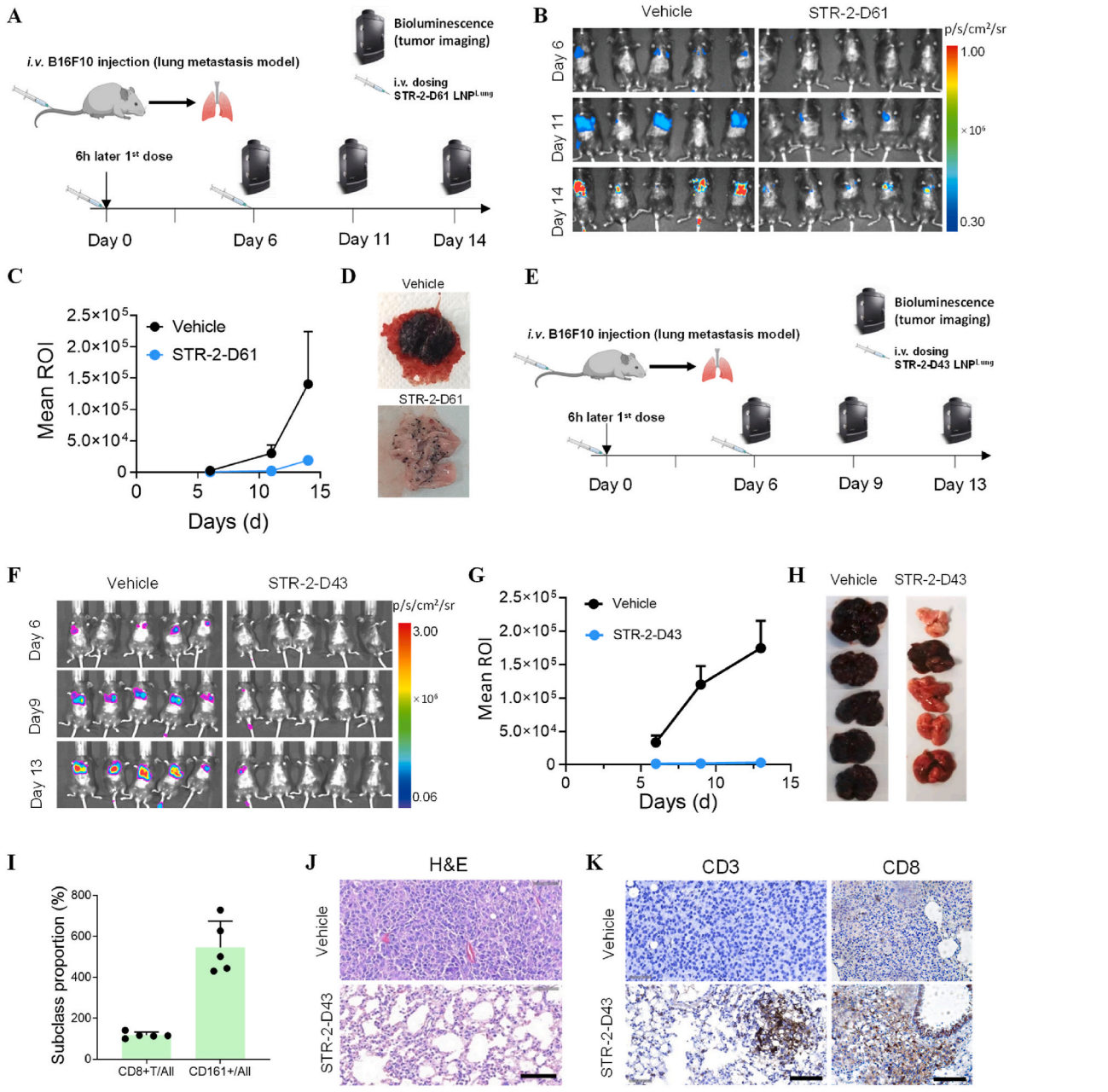

Fig. 5. The STR-2 variants LNP^{Lung} demonstrated extremely superior ability to inhibit lung metastatic tumor. (A) The schematic diagram of STR-2-D61 LNP^{Lung} for lung metastatic tumor therapy. Mice were inoculated intravenously with luciferase-expressing B16F10 and randomly divided into two groups. After 6 h, mice were *i.v.* injected twice with STR-2-D61 LNP^{Lung} at an mRNA dose of 1 mg/kg **(B, C)** Tumor growth of each group was monitored using *IVIS* system on day 6, 11, 14, and the data were quantitatively analyzed (n = 5 biologically independent animals). **(D)** The lung images indicated vehicle group had more obvious tumor lung metastasis compared to STR-2-D61 at day 14. **(E)** The antitumor effects of STR-2-D43 LNP^{Lung} against lung metastatic tumor was also evaluated through similar experiments as described above. **(F–H)** The *IVIS* imaging and lung tissue photographs demonstrated that STR-2-D43 LNP^{Lung} dramatically inhibited lung metastasis of tumor (n = 5 biologically independent animals). **(I, K)** The STR-2-D43 LNP^{Lung} not only significantly increased the proportion of CD161+ NK cells in blood, but also enhanced the infiltration of CD3+T cells and CD8$^+$ T cells in the lung. **(J)** H&E staining demonstrated that STR-2-D43 group had a close-to-healthy lung tissue (Scale bar = 100 μm). Data are illustrated as mean ± s.e.m. (n = 5 biologically independent animals).

treatment of lung cancer or lung metastasis by reducing IL-15 leakage.

To verify this, anti-tumor activity of STR-2-D61 LNP^{Lung} was explored in B16F10 lung metastatic tumor models. The C57BL/6 mice were firstly *i.v.* injected with luciferase-expressed B16F10 cells, then were treated by STR-2-D61 LNP^{Lung} at indicated days (Fig. 5A). At given time-points, mice were imaged by *in vivo* imaging system (IVIS). Compared with control group, STR-2-D61 LNP^{Lung} showed notable reduction or complete elimination of luciferase expression (Fig. 5B and 5C). This was also confirmed by isolated lung tissue images, in which lots of tumor lesions were observed in the vehicle group (Fig. 5D). Similar experiment was performed with STR-2-D43 LNP^{Lung} as well (Fig. 5E). STR-2-D43 LNP^{Lung} treated mice exhibited remarkable tumor inhibition detected by IVIS (Fig. 5F–H). The lung sections of hematoxylin and eosin (H&E) staining confirmed the anti-tumor efficacy that STR-2-D43 LNP^{Lung} group showed a close-to-healthy lung tissue (Fig. 5J). We further analyzed the numbers of cytotoxic T cells and natural killer (NK) cells in blood. The proportion of CD161+ (mouse NK cell marker) cells in blood were obviously increased in STR-2-D43 LNP^{Lung} group compared to vehicle group (Fig. 5I). Considering NK cell is one of the key target cells of IL-15 superagonist and plays key roles

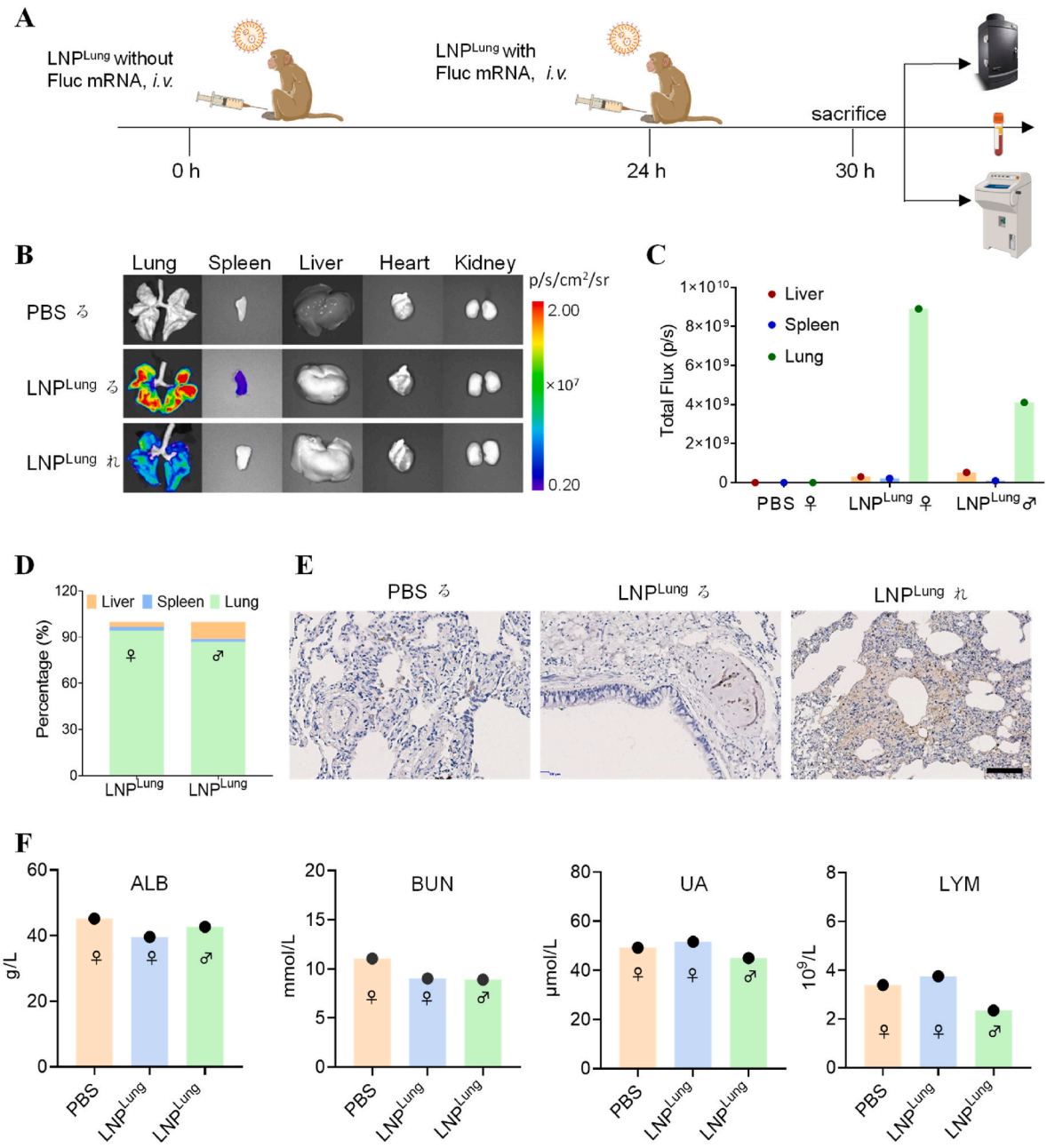

Fig. 6. Investigation on the delivery efficiency and bio-safety of mRNA-LNP^{Lung} in non-human primates (NHPs). (A) Schematic illustration of experimental protocol design in Macaca fasciculiris. One of female was treated with 1 × PBS, while the other female and male were administrated with Fluc mRNA-LNP^{Lung}. The experimental groups were administered twice via *i.v.* at 0 h (0.25 mg/kg) and 24 h (0.125 mg/kg), respectively. After another 6 h, major organs and blood were collected to explore the delivery efficiency and safety of mRNA-LNP^{Lung}. **(B–D)** The expression of Luc mRNA in major organs showed that LNP^{Lung} effectively delivered mRNA to lung with high specificity (94.46 % and 86.90 %). **(E)** Immunohistochemistry (IHC) analysis was employed to further verify the Luc mRNA expression in the lungs (Scale bar, 100 μm). **(F–I)** The blood parameters were served as assessment indicators to validate the bio-safety of mRNA-LNP^{Lung} *in vivo*. ALB: albumin, BUN: blood urea nitrogen, UA: urea, LYM: lymphocyte.

in tumor killing, this result indicated that the mRNA-LNP^{Lung} system could successfully activate its target cells. We also noticed the obvious increasing of lung infiltration of CD3+T cell and CD8^{+} T cell in STR-2-D43 group (Fig. 5K), which is another evidence of mRNA-LNP^{Lung} system induced activation on target cell. All of these results illustrated that STR-2 variants LNP^{Lung} achieved outstanding anti-tumor efficacy in lung metastasis tumor model by mobilization of local CD8+T cells and NK cells.

3.6. *Targeted delivery and safety evaluation of LNP^{Lung} in NHP*

To further evaluate the potential of clinical application using mRNA-LNP modality, a few experiments were conducted in non-human primate (NHP). We selected mRNA-LNP^{Lung} systems with i.v. administration into Macaca fascicularis, in which one female was treated by 1 × PBS, another female and a male were treated by Fluc mRNA-LNP^{Lung} (Fig. 6A). Two injections were completed at 0 h and 24 h, respectively. After another 6 h, NHPs were sacrificed and major tissues were imaged by IVIS. Compared with the control group, very strong luciferase expression in lungs were detected in both NHPs with almost

undetectable expression in the liver and spleen. The expression percent of the lungs reached 94.46 % and 86.90 %, respectively (Fig. 6B–D). Immunohistochemistry (IHC) analysis also confirmed that Fluc was expressed in the lungs, with significantly higher compared to the control group (Fig. 6E). These results fully demonstrated the efficiency and specificity of mRNA-LNP^{Lung} in NHPs. Meanwhile, we assessed the safety by analyzing several blood parameters, including albumin (ALB), blood urea nitrogen (BUN), urea (UA), and lymphocytes (LYM). All indicators are within normal range, no obvious difference compared with control group was observed (Fig. 6F), indicating well-tolerated feathers of mRNA-LNP^{Lung} in liver, kidney and immune system. Overall, these results demonstrated that LNP^{Lung} exhibited a promising lung targeting efficacy and safety in NHPs, resulting great potentials for clinical translation.

4. Discussion

As the National Cancer Institute's immunotherapy workshop in 2007 recognized the potential to revolutionize cancer treatment, the IL-15 has been widely acknowledged. Multiple clinical studies have been exploring the feasibility of IL-15 related agents as a potential anti-tumor therapy [63,64]. However, its dual effects from T/NK cell interaction raise concerns about on-target side effects, leading to inadvertent infiltration and attacks on non-tumor organs [65,66]. This issue arises from the activation of effector T cells and natural killer (NK) cells, whose cytokine production can exacerbate these effects [66]. Therefore, IL-15-based systemic therapies face challenges for dosage limitation during treatment. Considering these evidences, it is reasonable that maximizing IL-15 concentration in the tumor region and minimizing leakage into circulation may provide an attractive strategy for cancer treatment. In this work, the proof-of-concept (POC) experiments were performed based on our established mRNA-LNP platform (named STAR LNP) via targeted delivery of IL-15 superagonist mRNA for cancer therapy.

We optimized IL-15 superagonist structures and found that STR-2, with a C-terminal IL-15 structure, showed the best efficacy. We introduced D mutations to create STR-2-D61 and STR-2-D43 mRNAs, which demonstrated even better activity. Targeted delivery using LNP^{Local} and LNP^{Lung} effectively delivered mRNA to the target area and minimized systemic leakage, balancing efficacy and stress. Anti-tumor experiments confirmed that mRNA-LNP provided superior therapeutic effects with lower systemic exposure and negligible side effects compared to N-803, even at higher doses. We validated the delivery efficacy, specificity, and safety of mRNA-LNP^{Lung} in mice and non-human primates, suggesting potential for clinical translation in lung cancer therapy. Overall, this work offers a promising strategy for IL-15-based cancer therapy using targeted mRNA-LNP, balancing efficacy and systemic stress, and expanding the therapeutic window of IL-15 agents.

CRediT authorship contribution statement

Juntao Yu: Writing – original draft, Project administration, Methodology, Data curation. **Qian Li:** Writing – original draft, Project administration, Methodology, Data curation. **Chaoting Zhang:** Methodology, Resources, Visualization. **Qiu Wang:** Writing – review & editing, Project administration. **Shenggen Luo:** Project administration. **Xiaona Wang:** Project administration. **Rongkuan Hu:** Visualization, Supervision, Resources, Funding acquisition, Conceptualization. **Qiang Cheng:** Writing – review & editing, Writing – original draft, Visualization, Supervision, Conceptualization.

Declaration of competing interest

J.Y., S.L., X.W., and R.H. are employees and receive salary from Starna Therapeutics. Q.C. serves on the scientific advisory board and owns the stock of Starna Therapeutics. All other authors declare no competing interests. The patents have been filed relating to the data presented in this study.

Acknowledgements

We thank employees of Starna Therapeutics for their helpful technical and scientific support with NHPs and materials. This study was supported in part from Starna Therapeutics (STR-P002), Jiangsu Provincial Science and Technology Project (SBK2023070025), Suzhou Science and Technology Project (ZXL2023267), the ""Open Competition to Select the Best Candidates" Key Technology Program for Cell and Gene Therapy of NCTIB (NCTIB2023XB02001), the Fundamental Research Funds for the Central Universities, Peking University, and the Beijing Life Science Academy (2023000CC0040), and the Postdoctoral Fellowship Program of CPSF (GZC20240050). We are very grateful to Professor Wei Tuo from the Institute of Zoology, Chinese Academy of Sciences for the support of Biorender.

Appendix A. Supplementary data

Supplementary data to this article can be found online at https://doi.org/10.1016/j.biomaterials.2024.123047.

Data availability

Data will be made available on request.

References

[1] T.A. Fehniger, M.A. Caligiuri, Interleukin 15: biology and relevance to human disease, Blood 97 (1) (2001) 14–32.
[2] K. Yoshihara, T. Yajima, C. Kubo, Y. Yoshikai, Role of interleukin 15 in colitis induced by dextran sulphate sodium in mice, Gut 55 (3) (2006) 334–341.
[3] M. Desbois, C. Béal, M. Charrier, B. Besse, G. Meurice, N. Cagnard, et al., IL-15 superagonist RLI has potent immunostimulatory properties on NK cells: implications for antimetastatic treatment, J. Immunother. Cancer 8 (1) (2020).
[4] K.M. Knudson, J.W. Hodge, J. Schlom, S.R. Gameiro, Rationale for IL-15 superagonists in cancer immunotherapy, Expert Opin. Biol. Ther. 20 (7) (2020) 705–709.
[5] J.C. Steel, T.A. Waldmann, J.C. Morris, Interleukin-15 biology and its therapeutic implications in cancer, Trends Pharmacol. Sci. 33 (1) (2012) 35–41.
[6] W. Chen, N. Liu, Y. Yuan, M. Zhu, X. Hu, W. Hu, et al., ALT-803 in the treatment of non-muscle-invasive bladder cancer: preclinical and clinical evidence and translational potential, Front. Immunol. 13 (2022) 1040669.
[7] H. Furuya, O. Chan, I. Pagano, C. Zhu, N. Kim, R. Peres, et al., Effectiveness of two different dose administration regimens of an IL-15 superagonist complex (ALT-803) in an orthotopic bladder cancer mouse model, J. Transl. Med. 17 (1) (2019) 1–12.
[8] M. Ahdoot, D. Theodorescu, Immunotherapy of high risk non-muscle invasive bladder cancer, Expert Rev. Clin. Pharmacol. 14 (11) (2021) 1345–1352.
[9] G. Gakis, Adjuvant instillation therapy for non-muscle invasive bladder cancer-beyond BCG und mitomycin C, Aktuelle Urol. 53 (2) (2022).
[10] R. Romee, S. Cooley, M.M. Berrien-Elliott, P. Westervelt, M.R. Verneris, J. E. Wagner, et al., First-in-human phase 1 clinical study of the IL-15 superagonist complex ALT-803 to treat relapse after transplantation, Blood 131 (23) (2018) 2515–2527.
[11] Y. Peng, S. Fu, Q. Zhao, Update on the scientific premise and clinical trials for IL-15 agonists as cancer immunotherapy, J. Leukocyte Biol. 112 (4) (2022) 823–834, 2022.
[12] K. Margolin, C. Morishima, V. Velcheti, J.S. Miller, S.M. Lee, A.W. Silk, et al., Phase I trial of ALT-803, a novel recombinant IL15 complex, in patients with advanced solid tumors, Clin. Cancer Res. 24 (22) (2018) 5552–5561.
[13] Y. Guo, L. Luan, N.K. Patil, E.R. Sherwood, Immunobiology of the IL-15/IL-15Rα complex as an antitumor and antiviral agent. Cytokine Growth Factor, Rev 38 (2017) 10–21.
[14] K.M. Knudson, K.C. Hicks, Y. Ozawa, J. Schlom, S.R. Gameiro, Functional and mechanistic advantage of the use of a bifunctional anti-PD-L1/IL-15 superagonist, J. Immuno.Ther. Cancer 8 (1) (2020).
[15] K.M. Knudson, K.C. Hicks, S. Alter, J. Schlom, S.R. Gameiro, Mechanisms involved in IL-15 superagonist enhancement of anti-PD-L1 therapy, J. Immuno. Ther. Cancer 7 (1) (2019) 1–16.
[16] T.A. Waldmann, The biology of IL-15: implications for cancer therapy and the treatment of autoimmune disorders, J. Investing Dermatol. Symp. Proc. 16 (1) (2013) S28–S30.
[17] M.T. Williams, Y. Yousafzai, C. Cox, A. Blair, R. Carmody, S. Sai, et al., Interleukin-15 enhances cellular proliferation and upregulates CNS homing molecules in pre-B acute lymphoblastic leukemia, Blood 123 (20) (2014) 3116–3127.

[18] J. Chen, M. Petrus, R. Bamford, J.H. Shih, J.C. Morris, J.E. Janik, et al., Increased serum soluble IL-15Rα levels in T-cell large granular lymphocyte leukemia, Blood 119 (1) (2012) 137–143.

[19] R. Zhang, M.V. Shah, J. Yang, S.B. Nyland, X. Liu, J.K. Yun, et al., Network model of survival signaling in large granular lymphocyte leukemia, Proc. Natl. Acad. Sci. U.S.A. 105 (42) (2008) 16308–16313.

[20] R. Zambello, M. Facco, L. Trentin, R. Sancetta, C. Tassinari, A. Perin, et al., Interleukin-15 triggers the proliferation and cytotoxicity of granular lymphocytes in patients with lymphoproliferative disease of granular lymphocytes, Blood 89 (1) (1997) 201–211.

[21] M.K. Kennedy, M. Glaccum, S.N. Brown, E.A. Butz, J.L. Viney, M. Embers, et al., Reversible defects in natural killer and memory CD8 T cell lineages in interleukin 15–deficient mice, J. Exp. Med. 191 (5) (2000) 771–780.

[22] J.P. Lodolce, P.R. Burkett, D.L. Boone, M. Chien, A. Ma, T cell–independent interleukin 15rα signals are required for bystander proliferation, J. Exp. Med. 194 (8) (2001) 1187–1194.

[23] T.A. Waldmann, E. Lugli, M. Roederer, L.P. Perera, J.V. Smedley, R.P. Macallister, et al., Safety (toxicity), pharmacokinetics, immunogenicity, and impact on elements of the normal immune system of recombinant human IL-15 in rhesus macaques, Blood 117 (18) (2011) 4787–4795.

[24] C. Berger, M. Berger, R.C. Hackman, M. Gough, C. Elliott, M.C. Jensen, et al., Safety and immunologic effects of IL-15 administration in nonhuman primates, Blood 114 (12) (2009) 2417–2426.

[25] M.C. Sneller, W.C. Kopp, K.J. Engelke, J.L. Yovandich, S.P. Creekmore, T. A. Waldmann, et al., IL-15 administered by continuous infusion to rhesus macaques induces massive expansion of CD8+ T effector memory population in peripheral blood, Blood 118 (26) (2011) 6845–6848.

[26] E. Lugli, C.K. Goldman, L.P. Perera, J. Smedley, R. Pung, J.L. Yovandich, et al., Transient and persistent effects of IL-15 on lymphocyte homeostasis in nonhuman primates, Blood 116 (17) (2010) 3238–3248.

[27] N. Ibrahim, A. Barruchet, M.R. Moro, C. Blanchet, Severe neutropenia in an anorexic adolescent girl: a stigma of underfeeding syndrome? Eat. Weight Disord. 26 (4) (2021) 1271–1275.

[28] D. Gibson, P.S. Mehler, Anorexia nervosa and the immune system—a narrative review, J. Clin. Med. 8 (11) (2019) 1915.

[29] A. Saez, B. Herrero-Fernandez, R. Gomez-Bris, H. Sánchez-Martinez, J. M. Gonzalez-Granado, Pathophysiology of inflammatory bowel disease: innate immune system, Int. J. Mol. Sci. 24 (2) (2023) 1526.

[30] F. Di Vincenzo, A. Del Gaudio, V. Petito, L.R. Lopetuso, F. Scaldaferri, Gut microbiota, intestinal permeability, and systemic inflammation: a narrative review, Intern. Emerg. Med. 19 (2) (2024) 275–293.

[31] L. Lynch, A.E. Hogan, D. Duquette, C. Lester, A. Banks, K. LeClair, et al., iNKT cells induce FGF21 for thermogenesis and are required for maximal weight loss in GLP1 therapy, Cell metab. 24 (3) (2016) 510–519.

[32] J. Zhang, X.-Y. Wu, Jin, R.-M. Neutropenia, Diagnosis and management, World J. Pediatr. 18 (11) (2022) 771–777.

[33] ImmunityBio, ImmunityBio announces FDA acceptance of biologics license application for N-803 in BCG-unresponsive non-muscle-invasive bladder cancer carcinoma in situ, ImmunityBio Official Website, https://immunitybio.com/immunitybio-announces-fda-acceptance-of-biologics-license-application-for-n-803-in-bcg-unresponsive-non-muscle-invasive-bladder-cancer-carcinoma-in-situ/, 2022. (Accessed 28 June 2022).

[34] M. Gaviria, B. Kilic, A network analysis of COVID-19 mRNA vaccine patents, Nat. Biotechnol. 39 (5) (2021) 546–548.

[35] Y.-K. Kim, RNA therapy: rich history, various applications and unlimited future prospects, Exp. Mol. Med. 54 (4) (2022) 455–465.

[36] Y. Weng, C. Li, T. Yang, B. Hu, M. Zhang, S. Guo, et al., The challenge and prospect of mRNA therapeutics landscape, Biotechnol. Adv. 40 (2020) 107534.

[37] S. Chen, X. Huang, Y. Xue, E. Álvarez-Benedicto, Y. Shi, W. Chen, et al., Nanotechnology-based mRNA vaccines, Nat. Re. Methods Primers 3 (1) (2023) 63.

[38] Q. Chen, Y. Zhang, H. Yin, Recent advances in chemical modifications of guide RNA, mRNA and donor template for CRISPR-mediated genome editing, Adv. Drug Delivery Rev. 168 (2021) 246–258.

[39] H. Kwon, M. Kim, Y. Seo, Y.S. Moon, H.J. Lee, K. Lee, et al., Emergence of synthetic mRNA: in vitro synthesis of mRNA and its applications in regenerative medicine, Biomaterials 156 (2018) 172–193.

[40] X. Huang, N. Kong, X. Zhang, Y. Cao, R. Langer, W. Tao, The landscape of mRNA nanomedicine, Nat. Med. 28 (11) (2022) 2273–2287.

[41] Y. Zong, Y. Lin, T. Wei, Q. Cheng, Lipid nanoparticle (LNP) enables mRNA delivery for cancer therapy, Adv. Mater. (2023) 2303261.

[42] E. Kon, N. Ad-El, I. Hazan-Halevy, L. Stotsky-Oterin, D. Peer, Targeting cancer with mRNA–lipid nanoparticles: key considerations and future prospects, Nat. Rev. Clin. Oncol. (2023) 1–16.

[43] C. Liu, Q. Shi, X. Huang, S. Koo, N. Kong, W. Tao, mRNA-based cancer therapeutics, Nat. Rev. Cancer (2023) 1–18.

[44] S.H. Kiaie, N. Majidi Zolbanin, A. Ahmadi, R. Bagherifar, H. Valizadeh, F. Kashanchi, et al., Recent advances in mRNA-LNP therapeutics: immunological and pharmacological aspects, J. Nanobiotechnol. 20 (1) (2022) 276.

[45] L. Miao, L. Li, Y. Huang, D. Delcassian, J. Chahal, J. Han, et al., Delivery of mRNA vaccines with heterocyclic lipids increases anti-tumor efficacy by STING-mediated immune cell activation, Nat. Biotechnolo. 37 (10) (2019) 1174–1185.

[46] M. Ripoll, M.-C. Bernard, C. Vaure, E. Bazin, S. Commandeur, V. Perkov, et al., An imidazole modified lipid confers enhanced mRNA-LNP stability and strong immunization properties in mice and non-human primates, Biomaterials 286 (2022) 121570.

[47] T. Wei, Q. Cheng, L. Farbiak, D.G. Anderson, R. Langer, D.J. Siegwart, Delivery of tissue-targeted scalpels: opportunities and challenges for in vivo CRISPR/Cas-Based genome editing, ACS Nano 14 (8) (2020) 9243–9262.

[48] K.L. Swingle, H.C. Safford, H.C. Geisler, A.G. Hamilton, A.S. Thatte, M. M. Billingsley, et al., Ionizable lipid nanoparticles for in vivo mRNA delivery to the placenta during pregnancy, J. Am. Chem. Soc. 145 (8) (2023) 4691–4706.

[49] Q. Cheng, T. Wei, L. Farbiak, L.T. Johnson, S.A. Dilliard, D.J. Siegwart, Selective organ targeting (SORT) nanoparticles for tissue-specific mRNA delivery and CRISPR–Cas gene editing, Nat. Nanotechnol. 15 (4) (2020) 313–320.

[50] T. Wei, Y. Sun, Q. Cheng, S. Chatterjee, Z. Traylor, L.T. Johnson, et al., Lung SORT LNPs enable precise homology-directed repair mediated CRISPR/Cas genome correction in cystic fibrosis models, Nat. Commun. 14 (1) (2023) 7322.

[51] M. Qiu, Y. Tang, J. Chen, R. Muriph, Z. Ye, C. Huang, et al., Lung-selective mRNA delivery of synthetic lipid nanoparticles for the treatment of pulmonary lymphangioleiomyomatosis, Proc. Natl. Acad. Sci. USA 119 (8) (2022) e2116271119.

[52] L. Xue, A.G. Hamilton, G. Zhao, Z. Xiao, R. El-Mayta, X. Han, et al., High-throughput barcoding of nanoparticles identifies cationic, degradable lipid-like materials for mRNA delivery to the lungs in female preclinical models, Nat. Commun. 15 (1) (2024) 1884.

[53] G. Zeng, Z. He, H. Yang, Z. Gao, X. Ge, L. Liu, et al., Cationic lipid pairs enhance liver-to-lung tropism of lipid nanoparticles for in vivo mRNA delivery, ACS Appl. Mater. Interfaces 16 (20) (2024) 25698–25709.

[54] K. Su, L. Shi, T. Sheng, X. Yan, L. Lin, C. Meng, et al., Reformulating lipid nanoparticles for organ-targeted mRNA accumulation and translation, Nat. Commun. 15 (1) (2024) 5659.

[55] K.-p. Han, X. Zhu, B. Liu, E. Jeng, L. Kong, J.L. Yovandich, et al., IL-15: IL-15 receptor alpha superagonist complex: high-level co-expression in recombinant mammalian cells, purification and characterization, Cytokine 56 (3) (2011) 804–810.

[56] T.A. Waldmann, The biology of interleukin-2 and interleukin-15: implications for cancer therapy and vaccine design, Nat. Rev. Immunol. 6 (8) (2006) 595–601.

[57] S.R. Talbot, S. Biernot, A. Bleich, R.M. van Dijk, L. Ernst, C. Häger, et al., Defining body-weight reduction as a humane endpoint: a critical appraisal, Lab. Anim. 54 (1) (2020) 99–110.

[58] X. Zhu, W.D. Marcus, W. Xu, H.-i. Lee, K. Han, J.O. Egan, et al., Novel human interleukin-15 agonists, J. Immunol. 183 (6) (2009) 3598–3607.

[59] M. Cai, X. Huang, X. Huang, D. Ju, Y.Z. Zhu, L. Ye, Research progress of interleukin-15 in cancer immunotherapy, Front. Pharmacol. 14 (2023) 1184703.

[60] Y. Hailemichael, D.H. Johnson, N. Abdel-Wahab, W.C. Foo, S.-E. Bentebibel, M. Daher, et al., Interleukin-6 blockade abrogates immunotherapy toxicity and promotes tumor immunity, Cancer Cell 40 (5) (2022) 509–523, e506.

[61] M. Wang, X. Zhai, J. Li, J. Guan, S. Xu, Y. Li, et al., The role of cytokines in predicting the response and adverse events related to immune checkpoint inhibitors, Front. Immunol. 12 (2021) 2894.

[62] J. Guo, Y. Liang, D. Xue, J. Shen, Y. Cai, J. Zhu, et al., Tumor-conditional IL-15 pro-cytokine reactivates anti-tumor immunity with limited toxicity, Cell Res. 31 (11) (2021) 1190–1198.

[63] A.V. Hirayama, C.K. Chou, T. Miyazaki, R.N. Steinmetz, H.A. Di, S.P. Fraessle, et al., A novel polymer-conjugated human IL-15 improves efficacy of CD19-targeted CAR T-cell immunotherapy, Blood Adv 7 (11) (2023) 2479–2493.

[64] T.A. Waldmann, S. Dubois, M.D. Miljkovic, K.C. Conlon, IL-15 in the combination immunotherapy of cancer, Front. Immunol. 11 (2020) 868.

[65] Y. Yang, A. Lundqvist, Immunomodulatory effects of IL-2 and IL-15; implications for cancer immunotherapy, Cancers 12 (12) (2020) 3586.

[66] Y. Zhou, T. Husman, X. Cen, T. Tsao, J. Brown, A. Bajpai, et al., Interleukin 15 in cell-based cancer immunotherapy, Int. J. Mol. Sci. 23 (13) (2022) 7311.